World Journal of Critical Care Medicine

Submit a Manuscript: https://www.f6publishing.com

World J Crit Care Med 2025 September 9; 14(3): 101462

DOI: 10.5492/wjccm.v14.i3.101462

ISSN 2220-3141 (online)

MINIREVIEWS

Point of care ultrasound evaluation of cardio-cerebral coupling

Ignacio J Previgliano, Hatem Soliman Aboumarie, Francisco M Tamagnone, Pablo M Merlo, Fernando A Sosa, Jose Feijoo, Maria C Carruega

Specialty type: Critical care medicine

Provenance and peer review: Invited article; Externally peer reviewed.

Peer-review model: Single blind

Peer-review report's classification

Scientific Quality: Grade B, Grade C, Grade D, Grade D

Novelty: Grade B, Grade B, Grade C, Grade D

Creativity or Innovation: Grade A, Grade B, Grade B, Grade D

Scientific Significance: Grade B, Grade B, Grade C, Grade C

P-Reviewer: Al-Nimer MSM; Chen L; Li M

Received: September 14, 2024

Revised: February 16, 2025

Accepted: March 6, 2025

Published online: September 9, 2025

Processing time: 226 Days and 14.2 Hours

Ignacio J Previgliano, Department of Neurology, Asociacion Argentina de Ultrasonografia Critica, Buenos Aires 1426, Ciudad Autónoma de, Argentina

Ignacio J Previgliano, Asociacion Argentina de Ultrasonografia Critica research group, Asociacion Argentina de Ultrasonografia Critica, Buenos Aires 1426, Ciudad Autónoma de, Argentina

Hatem Soliman Aboumarie, Department of Anaesthetics and Intensive Care, Harefield Hospital, Royal Brompton and Harefield Hospitals, London UB9 6JH, United Kingdom

Francisco M Tamagnone, President Asociacion Argentina de Ultrasonografia Critica, Buenos Aires 1426, Ciudad Autónoma de, Argentina

Pablo M Merlo, Department of Cardiology, Asociacion Argentina de Ultrasonografia Critica, Buenos Aires 1426, Ciudad Autónoma de, Argentina

Fernando A Sosa, Department of Critical Care, Hospital Aleman, Buenos Aires 1426, Ciudad Autónoma de, Argentina

Jose Feijoo, Department of Research, Asociacion Argentina de Ultrasonografia Critica, Buenos Aires 1426, Ciudad Autónoma de, Argentina

Maria C Carruega, Department of Neurosonology, Asociacion Argentina de Ultrasonografia Critica, Buenos Aires 1426, Ciudad Autónoma de, Argentina

Co-first authors: Ignacio J Previgliano and Hatem Soliman Aboumarie.

Corresponding author: Ignacio J Previgliano, MD, Professor, Department of Neurology, Asociacion Argentina de Ultrasonografia Critica, 2676 Virrey Loreto, Buenos Aires 1426, Ciudad Autónoma de, Argentina. ipreviglianо@asaruc.org

Abstract

Cardio-cerebral coupling (CCC) refers to the dynamic interplay between cardiac function and cerebral blood flow, essential for maintaining hemodynamic stability. Disruptions in CCC are particularly relevant in critical care, where they can exacerbate primary and secondary brain injuries. Ultrasound-based techniques, including transcranial Doppler, transcranial color-coded Doppler, and echocardiography, provide non-invasive methods to assess this relationship at the bedside. This scoping review explores the pathophysiology of CCC, ultrasound methodologies for its evaluation, and its clinical relevance. Key mechanisms such as cerebral autoregulation and neurovascular coupling are discussed, along with

SHOUT
SHARE
IT

ultrasound-derived parameters like pulsatility index, resistance index, and cerebral perfusion pressure. While ultrasound is a valuable tool, its limitations include operator dependency and equipment variability. Emerging evidence suggests that ultrasound-guided protocols, including ultrasound-guided cardio-cerebral resuscitation protocol and ultrasound-guided brain injury treatment protocol, may improve resuscitation strategies and neurocritical care monitoring. Despite its potential, further research is necessary to standardize assessment methods and integrate ultrasound-based CCC evaluation into routine clinical practice. Ongoing multicenter studies are expected to provide robust evidence supporting its clinical utility in managing brain-injured patients.

Key Words: Cardio-cerebral coupling; Transcranial Doppler; Echocardiography; Cerebral blood flow physiology; Cardiovascular physiology; Cerebral autorregulation; Brain circulation assessment

©The Author(s) 2025. Published by Baishideng Publishing Group Inc. All rights reserved.

Core Tip: Cardio-cerebral coupling represents the dynamic interplay between cardiac function and cerebral blood flow regulation, crucial for maintaining hemodynamic stability. This article highlights the role of point-of-care ultrasound, including transcranial Doppler, transcranial color-coded Doppler, and echocardiography, in assessing cardio-cerebral coupling at bedside. Ultrasound-derived indices such as pulsatility index, resistance index, and cerebral perfusion pressure offer valuable insights into cerebral autoregulation. While ultrasound is a powerful tool, its clinical utility remains limited by operator dependency and methodological variability. Standardized protocols show promise in optimizing resuscitation strategies and neurocritical care. Further multicenter studies are needed to establish its role in routine clinical practice.

Citation: Previgliano IJ, Aboumarie HS, Tamagnone FM, Merlo PM, Sosa FA, Feijoo J, Carruega MC. Point of care ultrasound evaluation of cardio-cerebral coupling. *World J Crit Care Med* 2025; 14(3): 101462
URL: https://www.wjgnet.com/2220-3141/full/v14/i3/101462.htm
DOI: https://dx.doi.org/10.5492/wjccm.v14.i3.101462

INTRODUCTION

Cardio-cerebral coupling (CCC) refers to the dynamic interplay between cardiac activity and cerebral blood flow (CBF) regulation. This relationship has garnered significant attention in neuroscience and cardiovascular physiology due to its implications for autonomic nervous system function, cerebral perfusion, and overall cardiovascular health. While cardiac output (CO) plays a role in maintaining cerebral perfusion, autonomic regulation is a central mechanism ensuring the stability of CBF across various physiological and pathological states. A recent systematic review[1] of the literature on CCC analyzed 41 studies, including prospective studies, retrospective reviews, and clinical trials. Of these, only 5 were prospective studies, while the rest were observational or retrospective. None of the clinical trials were randomized or adequately controlled, and all were assessed as being of low quality and high risk of bias. Results were heterogeneous, with evidence both supporting and refuting a relationship between CO and CBF in normal and pathological cerebrovascular states. This variability underscores the need for robust methodologies and comprehensive frameworks to understand CCC more accurately. Given this controversy, our aim is to review the pathophysiology of CBF regulation, with a focus on the critical role of autonomic mechanisms. Additionally, we evaluate the potential of ultrasound, particularly point-of-care ultrasound (POCUS), as a non-invasive, dynamic tool to assess and monitor CCC. By addressing the limitations of existing research, we aim to provide a clearer understanding of this complex interaction and its clinical implications.

PATHOPHYSIOLOGY OF CBF

Although the brain accounts for only 2% of body weight, it consumes 12% of CO, underscoring its critical role in regulating all body functions. This vital relationship defines both life and death: Respiratory arrest, whether under cardiopulmonary or neurological criteria, indicates damage to the medulla oblongata, where the respiratory center resides. The existence of CCC becomes almost rhetorical when viewed through the lens of CBF, which is one of physiology's most tightly regulated constants. To maintain this constancy, several regulatory mechanisms interact dynamically.

Autoregulation

CBF remains constant across a range of cerebral perfusion pressures (CPP). Autoregulation ensures this by adjusting vascular resistance in response to changes in mean arterial pressure (MAP) or intracranial pressure (ICP).

Chemoregulation

The chemoregulation includes: (1) Cerebral metabolic rate of oxygen consumption**:** Increased metabolic demand triggers vasodilation to enhance oxygen delivery; (2) Partial oxygen pressure: Hypoxia promotes cerebral vasodilation to optimize oxygen delivery; (3) Partial carbon dioxide pressure (PCO_2): Elevated PCO_2 causes vasodilation, while decreased PCO_2 induces vasoconstriction; and (4) PH: Changes in arterial pH, influenced by CO_2 levels, modulate vascular tone to stabilize CBF.

Neuronal regulation

The neuronal regulation includes: (1) Neurovascular coupling: Localized neuronal activity triggers vasodilation in adjacent vessels, ensuring oxygen and nutrient delivery match metabolic demands; (2) Muscle metaboreflex: During exercise, neural reflexes coordinate systemic and cerebral perfusion to prevent circulatory collapse; and (3) Endothelium-dependent regulation: The neurovascular unit (NVU), composed of endothelial cells, astrocytes, pericytes, and neurons, orchestrates dynamic vascular responses to maintain CBF. Endothelium-derived factors like nitric oxide play a crucial role in vasodilation.

CEREBRAL CIRCULATION, ICP, AND CEREBRAL AUTOREGULATION

The cranial vault is an inextensible compartment where brain parenchyma, blood, cerebrospinal fluid (CSF), and extracellular fluid interact dynamically to maintain cerebral homeostasis. According to the Monro-Kellie doctrine, ICP results from changes in intracranial volumes within this closed system. Consequently, any increase in the volume of one component requires compensatory reductions in the others to maintain ICP. This principle forms the foundation of modern understanding of intracranial dynamics and cerebral pathophysiology (Figure 1A).

Compensatory mechanisms in pathological conditions

In pathological conditions, such as the presence of a mass lesion (*e.g.*, tumor and hematoma) or edema, compensatory mechanisms are activated sequentially to preserve ICP: (1) CSF displacement: CSF shifts from the intracranial space to the spinal subarachnoid space; (2) Cerebral blood volume (CBV) reduction: Blood is displaced from the intracranial vasculature, reducing CBV before affecting CBF; and (3) Brain tissue displacement: When compensatory mechanisms fail, herniation may occur. These mechanisms explain why ICP remains stable despite volume changes until a critical threshold is reached, beyond which ICP rises abruptly (Figure 1B)[2].

CPP and Poiseuille's law

CPP is a critical determinant of CBF and can be defined as: CPP = MAP - ICP. In pathological states, ICP often replaces cerebrovascular resistance as the limiting factor for perfusion, making CPP highly dependent on ICP. Poiseuille's law further explains the factors influencing blood flow: $F = (8 \times \Delta P \times r^4)/(\pi \times \eta \times L)$, where F is blood flow, ΔP is the pressure gradient, r^4 is the vessel radius raised to the fourth power, π is the constant, η is viscosity, and L is vessel length. Simplified for cerebral circulation: $CBF = CPP \times r/\eta$. This underscores the importance of vessel radius in regulating CBF. Under normal conditions, autoregulation maintains CBF constant across CPP values of 60-120 mmHg (Figure 2A). However, in pathological states, autoregulation may fail, making CBF directly proportional to CPP (Figure 2B).

As long as vessels can adjust their diameter, vascular changes predominantly govern CBF. However, at the extremes of autoregulation, CBF becomes directly proportional to CPP. Alongside changes in vessel radius, CBV also fluctuates significantly, which plays a critical role in the development of intracranial hypertension. When examining the portion of the curve labeled vasoparalysis, vessels remain maximally dilated until they lose their pressure-dependent properties and transition back into the autoregulatory range. Under pathological conditions, this curve shifts to the right, necessitating higher MAP and CPP to restore autoregulation. A reduction in CBF to 35 mL/100 g/minute is generally tolerated by cerebral tissue without ischemic symptoms. However, once CBF decreases to 30 mL/100 g/minute or below, ischemic symptoms begin to emerge and progress (Figure 2C). Another variable that significantly impacts vessel diameter is hypoxia. The thresholds for hypoxia are even more permissive than those for CBF (Figure 2D). An increase in PCO_2 leads to an increase in CBF, while a decrease in PCO_2 reduces CBF. A similar inverse relationship applies to pH. This dynamic is crucial for maintaining proper cerebral perfusion pressure and oxygenation (Figure 2E).

Rosner's contribution: The vasodilator and vasoconstrictor cascades

Building on Becker's pioneering work on ICP dynamics, Rosner *et al*[3-5] advanced the field by introducing the vasodilator cascade, which elucidates the pathophysiological changes leading to secondary brain injuries: (1) A drop in CPP triggers compensatory vasodilation to maintain CBF; (2) Prolonged vasodilation increases CBV and ICP, further reducing CPP; and (3) This cycle perpetuates ischemia, contributing to cerebral damage. The vasodilator cascade (Figure 3A and B) provides a framework for understanding the transition from primary to secondary brain injuries. Rosner *et al*'s insights[3-5] into the relationship between CPP, CBF, and ICP redefined therapeutic strategies, emphasizing the critical importance of maintaining adequate CPP to prevent ischemia.

Rosner *et al*[3-5] also proposed the vasoconstrictor cascade (Figure 3C) and the complex vasoconstrictor cascade (Figure 3D), which complements the vasodilator cascade by explaining how therapeutic interventions, largely pioneered by Becker[6], mitigate intracranial hypertension and restore cerebral perfusion: (1) Hypertensive therapy: Increases MAP to restore CPP and prevent ischemia; (2) Mannitol: Decreases viscosity, reduces swelling, and improves oxygen delivery;

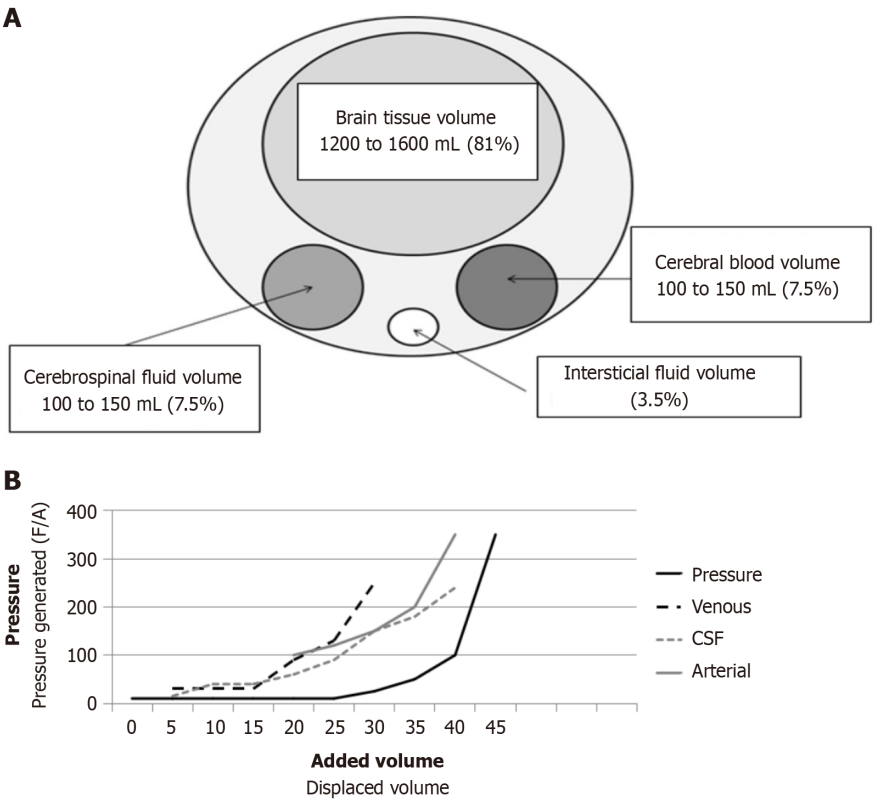

Figure 1 Maintain the intracranial pressure. A: Monro-Kellie law. Brain compartments with their respective volumes and percentage of total volume; B: Langfitt's pressure-volume curve showing the delay in pressure increase relative to volume increase, which suggests the existence of a compensatory mechanism. The generated pressure, calculated as force/area, is a consequence of the displaced volume. Firstly, the first capacitance system, the venous volume, is displaced, followed by the cerebrospinal fluid, and finally the arterial volume. F/A: Force/area; CSF: Cerebrospinal fluid.

and (3) Hyperventilation: Lowers PCO_2, inducing vasoconstriction and reducing ICP. The vasoconstrictor cascade integrates these therapeutic modalities into a unified framework, demonstrating their mechanisms of action in reversing secondary brain injuries. However, their application must be carefully tailored to individual patients to avoid exacerbating other pathologies.

Rosner *et al*'s CPP model[3-5] has sparked significant debate in the literature. For example: Chan *et al*[7] found that a CPP of 75 mmHg is sufficient to maintain adequate CBF using arteriojugular oxygen difference and transcranial Doppler (TCD) measurements. On the other hand Bouma *et al*[8] showed that patients with impaired autoregulation may require CPPs greater than 90 mmHg for sufficient perfusion. These contributions have resulted in modern traumatic brain injury (TBI) guidelines recommending a CPP target of 60 to 70 mmHg when autoregulation is intact[9]. As well as the importance of individualized strategies for managing CPP and emphasize the need for further research to refine thera-peutic targets.

NEURONAL AUTOREGULATION

Since the original description of the metabolic regulation theory by Roy and Sherrington[10] in 1890, it has been established that an increase in the concentration of metabolic byproducts (*e.g.*, H^+, K^+, and adenosine) leads to an increase in CBF. However, this theory does not fully explain the rapid, instantaneous changes in CBF observed in specific situations, such as the response described in Selye's general adaptation syndrome. This gap suggests the possibility that neurogenic stimuli, mediated by perivascular nerve endings, serves as rapid initiators of dynamic adjustments in CBF to meet metabolic demands. Once these adjustments are made, metabolic and chemical factors ensure their maintenance.

Perivascular nerve endings, identified in the outer layer of smooth muscle in cerebral arteries, arterioles, and veins, play a crucial role in this process. These nerve endings contain axons enriched with various neurotransmitters stored in synaptic vesicles. Stimulation of these nerves increases the release of neurotransmitters into the neuromuscular synaptic clefts of cerebral vascular smooth muscle, near receptor sites located on the vessel walls. Despite accumulating experimental evidence, the role of neural control in cerebrovascular regulation remains underestimated in much of the medical literature[11-13].

Peripheral pathways to cerebral vessels

Peripheral pathways involved in neuronal control of cerebral vessels include the sympathetic, parasympathetic, trigemino-vascular, and sensory (somatosensory and sensory organ) systems. Sympathetic fibers reach cerebral arteries

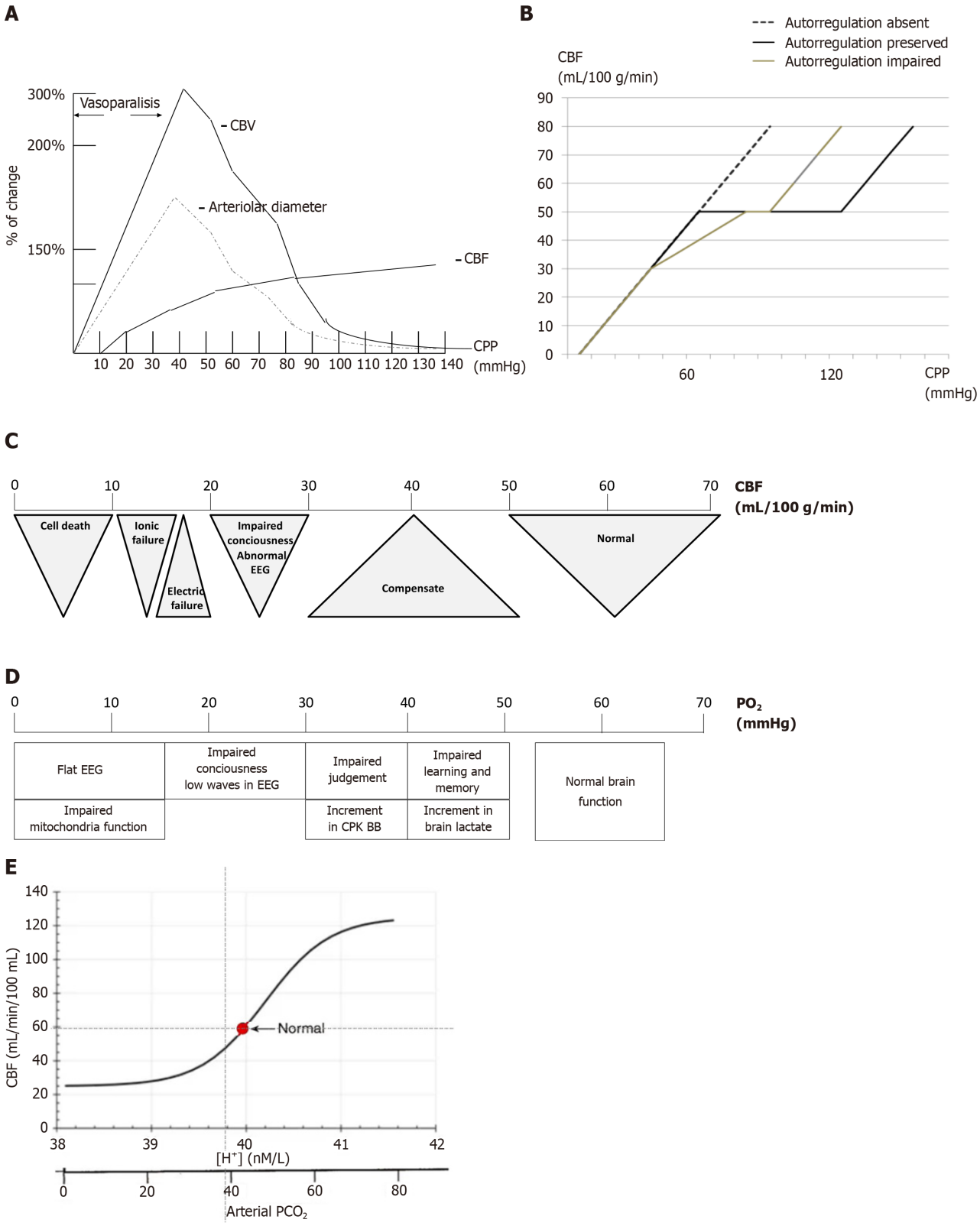

Figure 2 Relationship between cerebral blood flow and cerebral perfusion pressures. A: Solid line represents preserved autoregulation, dashed line represents impaired autoregulation, and dotted line represents abolished autoregulation. Note that both altered and abolished autoregulation require higher cerebral perfusion pressures to maintain adequate cerebral blood flow; B: Relative changes in cerebral blood volume, vascular diameter, and cerebral blood flow in response to changes in cerebral perfusion pressures; C: Cerebral blood flow thresholds. The critical threshold for cellular death is below 10 mL/100 g/minute; D: Hypoxic thresholds. Clinical neurological signs emerge only at significantly low partial oxygen levels (below 40 mmHg); E: A typical graph illustrating this relationship places cerebral blood flow on the y-axis and partial carbon dioxide pressure and pH on the x-axis. As partial carbon dioxide pressure and H^+ concentrations increase, cerebral blood flow (CBF) rises sharply until it reaches a plateau, beyond which further increases have a diminishing impact on CBF. Conversely, as partial carbon dioxide pressure and H^+ concentrations decrease, CBF declines until it reaches a lower plateau, where additional decreases have minimal effect on CBF. CBV: Cerebral blood volume; CBF: Cerebral blood flow; CPP: Cerebral perfusion pressures; PO_2: Partial oxygen; PCO_2: Partial carbon dioxide pressure; EEG:

Electroencephalography; CPK BB: Brain creatin phosphokinase.

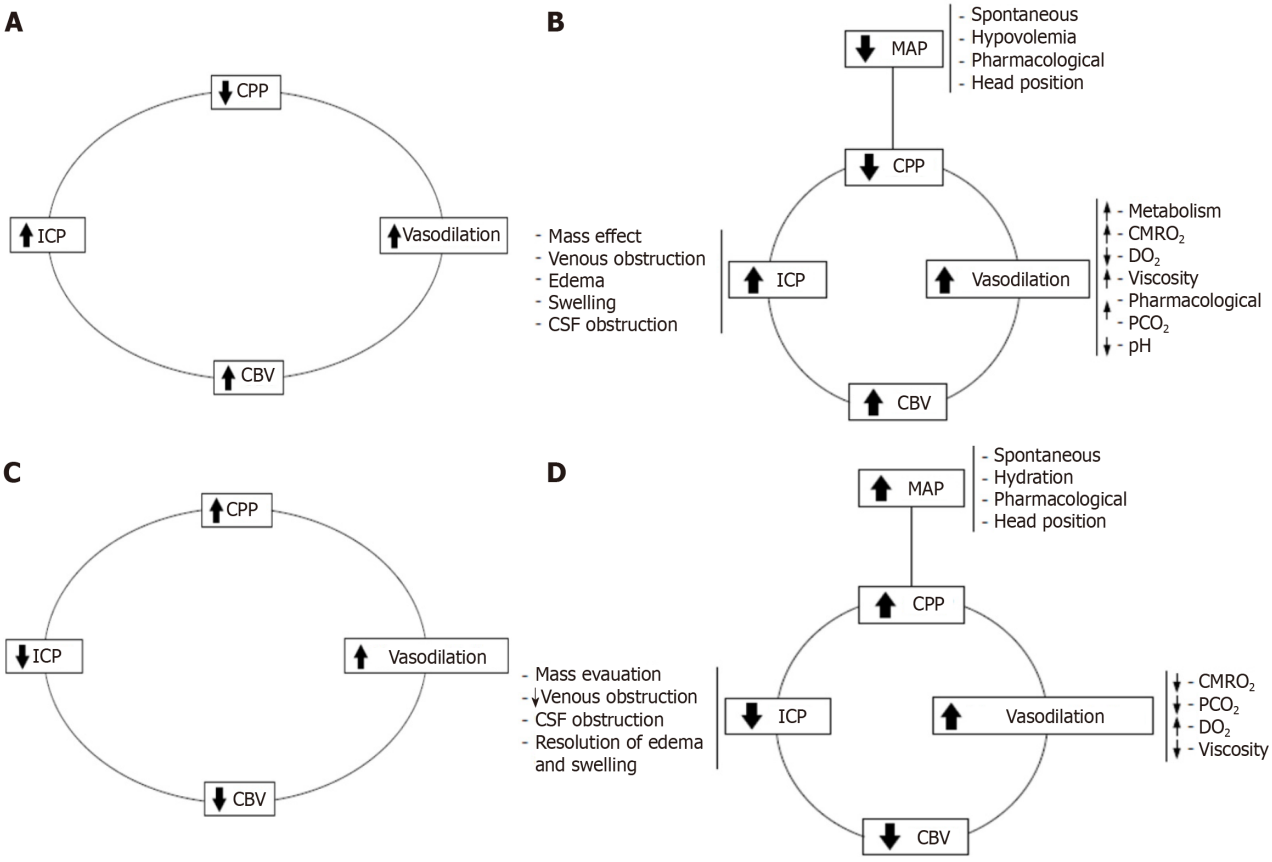

Figure 3 The vasodilator and vasoconstrictor cascades. A: Vasodilator cascade. A decrease in cerebral perfusion pressures (CPP) triggers vasodilation as a compensatory mechanism to maintain cerebral blood flow. It is evident that vasodilation increases cerebral blood volume, which, according to the Monro-Kellie doctrine, raises intracranial pressure (ICP). This rise in ICP further reduces CPP, creating a self-perpetuating vicious cycle; B: Complex vasodilator cascade. This framework helps clarify many seemingly contradictory events and illustrates how the cycle can be initiated by any of its primary components; C: Vasoconstrictor cascade. With constant levels of partial carbon dioxide pressure, cerebral metabolic rate of oxygen consumption, and related variables, an increase in CPP induces vasoconstriction, which reduces cerebral blood volume and ICP, thereby enhancing CPP. This mechanism is effective only if the patient is within or near their autoregulatory range; D: Complex vasoconstrictor cascade. Management strategies can target any single component of the cascade or employ a combination of multiple components for optimal effect. CPP: Cerebral perfusion pressures; ICP: Intracranial pressure; CBV: Cerebral blood volume; MAP: Mean arterial pressure; CSF: Cerebrospinal fluid; $CMRO_2$: Cerebral metabolic rate of oxygen; PCO_2: Partial carbon dioxide pressure; DO_2: Oxygen delivery.

via three distinct routes: (1) Carotid territory innervation: Postganglionic fibers from the superior cervical ganglion innervate vessels in the carotid system; (2) Vertebrobasilar territory innervation: Fibers originating from the stellate ganglion innervate the vertebrobasilar system; and (3) Rostral circle of Willis innervation: Fibers from the stellate ganglion travel along the common and internal carotid arteries to innervate the rostral part of the circle of Willis. Sympathetic innervation is denser in arteries arising from the internal carotid system compared to the vertebral system. This distribution aligns with the structure of tight junctions in the blood-brain barrier. Notably, 60%-90% of arterioles in regions such as the medial geniculate body, parietal and temporal cortices, caudate nucleus, inferior colliculus, thalamus, and hypothalamus are innervated. By contrast, only 10%-30% of arterioles in the brainstem, occipital cortex, and cerebellum receive sympathetic innervation.

The differences in sympathetic innervation between the anterior and posterior circulation have significant clinical implications. For example, posterior reversible encephalopathy syndrome and eclampsia provide indirect evidence of these differences. Anatomical and radiological findings in these conditions suggest that the posterior circulation, with its lower density of sympathetic innervation, has a reduced vasoconstrictor response to blood pressure increases. This reduced response predisposes the posterior circulation to vasogenic edema formation under conditions of elevated blood pressure.

MUSCLE METABOREFLEX

The muscle metaboreflex is a remarkable example of CCC, enabling precise hemodynamic regulation during exercise to

maintain homeostasis. Since its initial description by Alam and Smirk[14] in 1937, extensive research has elucidated its physiological basis. Reviews by Kaufman and Hayes[15], Teixeira and Vianna[16], Crisafulli[17], and Smith and Ainslie [18] provide some of the most comprehensive accounts of this phenomenon. During physical activities such as running, cycling, and rowing, large muscle groups are activated, leading to significant vasodilation within the working muscles due to the accumulation of metabolic byproducts. This process, termed functional sympatholysis, occurs as local metabolite production (*e.g.*, H^+, K^+, and adenosine) counteracts the generalized increase in sympathetic tone induced by exercise, thereby reducing systemic vascular resistance. Although this vasodilation has the potential to lower blood pressure, healthy individuals rely on compensatory mechanisms, such as an increase in CO, to maintain MAP at stable or slightly elevated levels.

Neural mechanisms governing the muscle metaboreflex

This precise hemodynamic regulation is achieved through a combination of neural mechanisms that ensure sufficient blood flow to active muscles while stabilizing MAP. Three primary mechanisms contribute to this cardiovascular adjustment: (1) Exercise pressor reflex: Peripheral feedback from mechanoreceptors and metaboreceptors in the working muscles adjusts autonomic activity to meet metabolic demands; (2) Central command: Signals originating in motor regions of the brain set a baseline level of sympathetic activation and vagal withdrawal proportional to exercise intensity; and (3) Arterial baroreflex: This reflex modulates blood pressure by integrating input from baroreceptors to maintain systemic hemodynamic stability. The medulla oblongata, which houses the key cardiovascular control nuclei, integrates and processes signals from these mechanisms to coordinate blood pressure and cardiovascular function. Central command establishes a baseline level of autonomic activity based on exercise intensity, which is further fine-tuned by feedback from the exercise pressor reflex and baroreceptors.

The role of the exercise pressor reflex: The exercise pressor reflex is mediated by sensory signals transmitted *via* thinly myelinated group III and unmyelinated group IV afferent fibers. Group III fibers are activated by mechanical distortion in the muscle, such as stretching or contraction. Group IV fibers respond to the accumulation of metabolic byproducts (*e.g.*, H^+, lactate, and CO_2) generated during muscle activity. This feedback loop ensures dynamic adjustments in autonomic activity and adrenal epinephrine release, which collectively regulate key hemodynamic parameters, including myocardial contractility, stroke volume, systemic vascular resistance, and heart rate (HR). Figure 4 illustrates how these mechanisms interact to maintain cardiovascular stability during exercise[19].

Impact on respiratory function: The muscle metaboreflex also plays a significant role in regulating respiratory function, particularly during intense or prolonged exercise. Increased sympathetic activity resulting from the metaboreflex enhances respiratory rate and depth (hyperventilation) to improve oxygen delivery to active muscles and facilitate the removal of CO_2 and other metabolic byproducts. In addition to this reflexive response, central command coordinates ventilation with the metabolic demands of exercise. This ensures that arterial blood gas homeostasis is maintained, supporting efficient oxygen delivery and CO_2 elimination[20].

ENDOTHELIUM-DEPENDENT REGULATION

The NVU provides a conceptual framework that links microvasculature to neuronal function and their joint responses to injury. The NVU is a dynamic structure composed of endothelial cells, which are bound by a basement membrane (forming the blood-brain barrier) and surrounded by astrocyte end-feet, pericytes, oligodendrocytes, microglial cells, and neurons. Figure 5 illustrates the structure and function of the NVU. First described by Harder *et al*[21] in 2002, the NVU is defined as a composite structure formed by neurons, interneurons (*e.g.*, oligodendrocytes and microglia), astrocytes, smooth muscle cells, pericytes, endothelial cells, and an extracellular matrix supported by a basement membrane[22,23]. These components are intricately and reciprocally connected, creating an anatomical and functional entity. This "whole" fulfills critical roles in: (1) Serving as a barrier separating the brain from systemic circulation and its components; (2) Regulating CBF; and (3) Facilitating substance exchange, immune surveillance, and trophic support[24].

Characteristics of brain endothelial cells

Brain endothelial cells differ significantly from systemic endothelial cells in several ways: (1) Tight Junctions: These cells form intercellular tight junctions and adherens junctions, regulated by protein complexes such as occludins and claudins. These junctions are linked to the cytoskeleton by accessory proteins like zonula occludens. Tight junctions determine the permeability and high electrical resistance characteristic of the blood-brain barrier, making it vulnerable to insults. Although gap junctions are also present, their precise function remains unclear; (2) Low pinocytosis and paracellular diffusion: Brain endothelial cells exhibit minimal pinocytosis and restricted paracellular diffusion of hydrophilic compounds; (3) High mitochondrial density: These cells have a large number of mitochondria, reflecting their high metabolic activity; and (4) Polarized membrane receptors and transporters: Brain endothelial cells express polarized receptors and transporters that actively mediate nutrient passage into the brain.

NVU and neurovascular coupling

Unlike cerebral autoregulation, which maintains CBF constancy under varying systemic pressures, the NVU is central to neurovascular coupling. Neurovascular coupling is a dynamic process characterized by robust vascular responses to vasoactive signals released during local increases in neuronal activity. These mechanisms are the foundation of functional

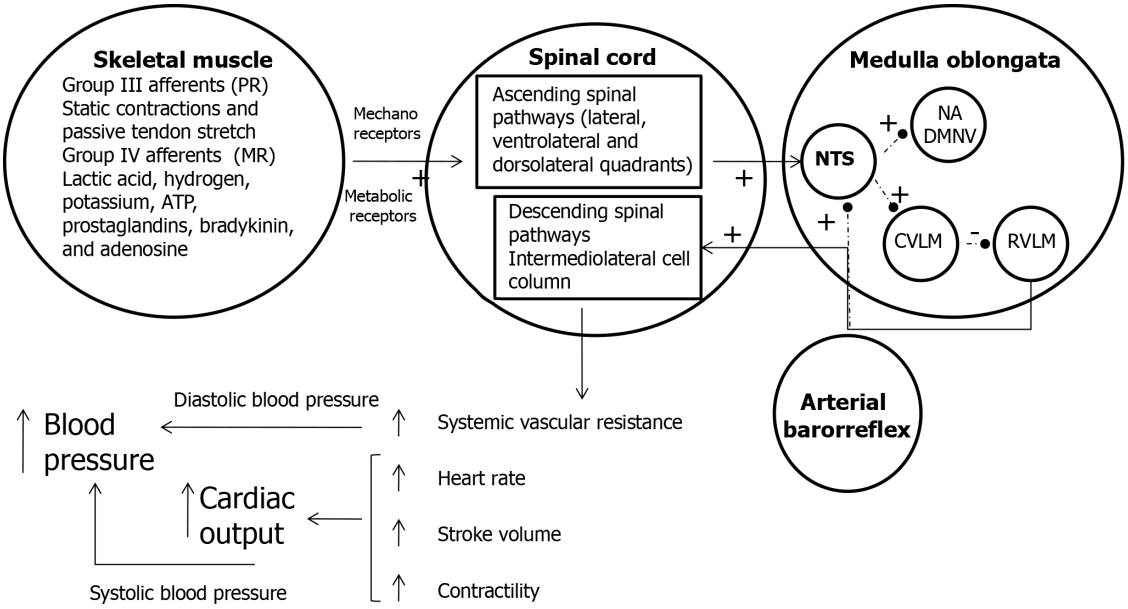

Figure 4 The combined action of the muscle metaboreflex, central command, and baroreceptors in cardiovascular regulation during exercise. Upon the initiation of exercise, type III afferent fibers are stimulated by static muscle contraction and passive tendon stretch through mechanoreceptors (pressure response), while type IV afferent fibers are activated by the accumulation of metabolic byproducts. Ascending spinal pathways, mediated by various neurotransmitters, then stimulate the nucleus tractus solitarius (NTS) in the brainstem, generating an inhibitory response. Under normal conditions (indicated by dotted lines), the NTS regulates parasympathetic activity *via* the nucleus ambiguous and dorsal motor nucleus of the vagus, as well as sympathetic activity *via* the caudal ventrolateral medulla and rostral ventrolateral medulla (RVLM), in response to arterial baroreflex stimulation. When the NTS is inhibited, this leads to stimulation of the RVLM and inhibition of the nucleus ambiguus, dorsal motor nucleus of the vagus, and caudal ventrolateral medulla. Stimulation of the RVLM activates the intermediolateral cell column, which results in an increase in systemic vascular resistance, along with enhanced stroke volume, heart rate, and myocardial contractility. Together, these changes increase cardiac output. The rise in systemic vascular resistance contributes to an increase in diastolic pressure, while the augmentation of cardiac output raises systolic blood pressure. This integrated response ensures the maintenance of hemodynamic stability during exercise. PR: Pressure reflex; MR: Metabolic reflex; NTS: Nucleus tractus solitarius; NA: Nucleus ambiguous; DMNV: Dorsal motor nucleus of the vagus; CVLM: Caudal ventrolateral medulla; RVLM: Rostral ventrolateral medulla.

hyperemic responses, enabling the rapid and precise redirection of blood flow to areas of heightened neuronal activity. This rapid vascular adjustment ensures that active brain regions receive an uninterrupted supply of oxygen and nutrients, supporting both viability and ongoing functions. NVU's role in this process highlights its critical importance in maintaining brain health and its susceptibility to injury or dysfunction[25].

PATHOPHYSIOLOGY OF THE CARDIOVASCULAR SYSTEM

Arterial blood pressure is the primary determinant of adequate organ perfusion. It is composed of several parameters: (1) Systolic blood pressure (SBP): The highest pressure exerted on arterial walls during cardiac systole (contraction), representing the force generated by the heart as it pumps blood into the arteries; (2) Diastolic blood pressure (DBP): The lowest pressure exerted on arterial walls during diastole (relaxation), representing the residual pressure in the arteries as the heart fills with blood; (3) Pulse pressure: The difference between SBP and DBP, reflecting stroke volume and arterial elasticity; and (4) MAP: The average pressure in the arteries throughout the cardiac cycle, calculated as: MAP = DBP + 1/3 (SBP - DBP). MAP represents the driving pressure for blood flow to organs and tissues during both systole and diastole, serving as a crucial indicator of tissue perfusion and oxygen delivery.

Determinants of arterial pressure

Several factors influence arterial pressure: (1) CO: The volume of blood ejected by the heart per minute, calculated as the product of stroke volume (SV) and HR. MAP is directly proportional to CO; an increase in CO elevates arterial pressure; (2) Systemic peripheral resistance (SPR): The resistance to blood flow in the systemic circulation. Higher SPR increases arterial pressure; (3) SV: The volume of blood ejected by the heart with each contraction, determined by the difference between end-diastolic and end-systolic volumes. Changes in SV directly affect arterial pressure; (4) Arterial elasticity and compliance: The ability of arteries to stretch and recoil helps buffer pressure fluctuations, maintaining steady MAP. Reduced elasticity (*e.g.*, in arteriosclerosis) raises arterial pressure; (5) Blood viscosity: Higher viscosity (*e.g.*, due to increased hematocrit or plasma proteins) increases resistance to flow, elevating arterial pressure; and (6) Sympathetic nervous system activity: The sympathetic nervous system regulates arterial pressure by modulating HR, contractility, and vascular tone *via* neurotransmitters. Key mechanisms include: (1) Baroreceptors: Located in the carotid sinuses and aortic arch, these stretch-sensitive receptors monitor changes in arterial pressure and trigger adjustments in parasympathetic

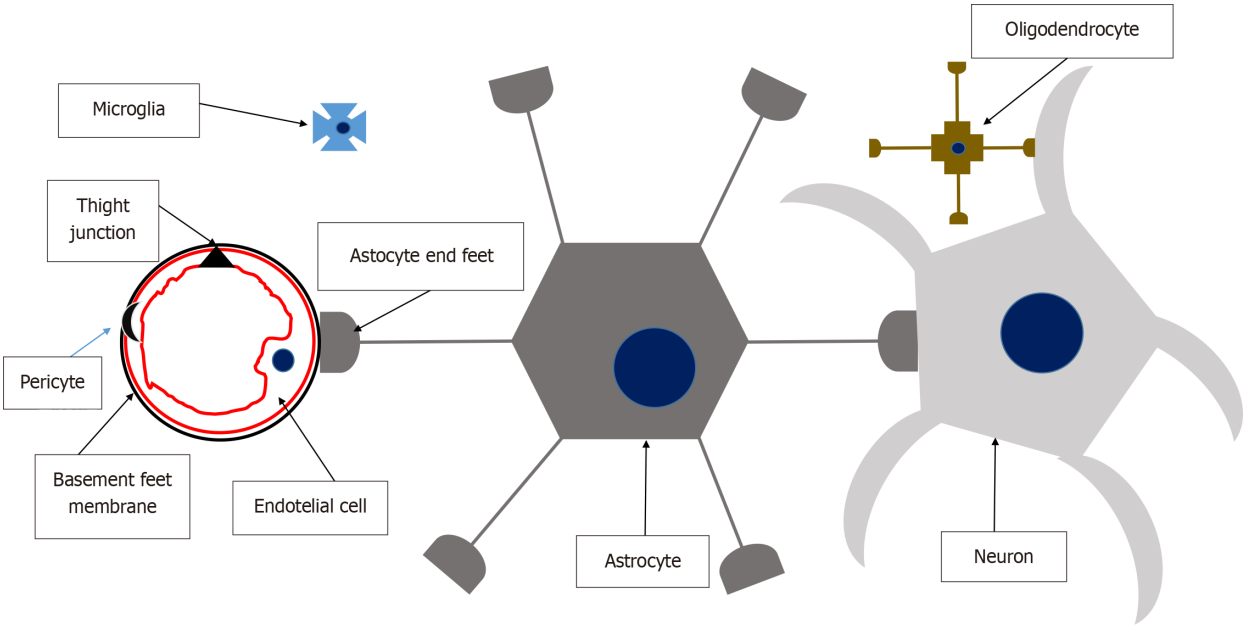

Figure 5 Neurovascular unit. Cerebral endothelial cells form tight junctions that seal the paracellular aqueous diffusion pathways between cells, maintaining the integrity of the blood-brain barrier. Pericytes are discontinuously distributed along capillaries, positioned between the endothelium and the basement membrane, which forms a specialized extracellular matrix distinct from the astrocytic foot processes that encase it. Astrocytes play a pivotal role as a bridge between neurons and the endothelial complex, facilitating the passage of vasoactive peptides that regulate vascular dilation or constriction. Microglia serve as the immunocompetent cells of the neurovascular unit, providing immune surveillance. Solutes cross the blood-brain barrier through passive diffusion, driven by concentration gradients and lipophilicity, or *via* facilitated transport mechanisms involving active or passive transport through endothelial cells.

and sympathetic activity to stabilize blood pressure. Increased pressure stimulates parasympathetic activity, decreasing HR, contractility, and vasoconstriction, while decreased pressure has the opposite effect; (2) Chemoreceptors: Located in the carotid and aortic bodies and medulla oblongata, these receptors respond to changes in oxygen, PCO_2, and pH. Hypoxemia or hypercapnia stimulates sympathetic activity, increasing HR, contractility, and vasoconstriction to improve tissue oxygenation and CO_2 elimination; (3) Renal regulation: The kidneys regulate arterial pressure through fluid and electrolyte balance, the renin-angiotensin-aldosterone system, and renal blood flow adjustments; and (4) Hormonal influence: Hormones such as angiotensin II, aldosterone, antidiuretic hormone, and atrial natriuretic peptide regulate vascular tone, fluid balance, and renal function, impacting arterial pressure.

MAP-centric pathophysiological framework

This pathophysiological model, which emphasizes MAP and its determinants (CO, SPR, SV, and sympathetic regulation), contrasts slightly with the Castle-Kirszbaum *et al*[1] framework, which focuses primarily on CO. While Castle-Kirszbaum *et al*[1] state that "direct evidence of how the simultaneous acute changes in CO and CBF are mediated by the sympathetic nervous system is lacking", our approach offers a more comprehensive explanation rooted in a broader physiological understanding. In our view, acute changes in CBF due to variations in CO can be better explained by integrating the contributions of SPR, MAP, and neurogenic regulation, highlighting the complexity of cardiovascular control mechanisms.

ASSESSMENT OF CCC THROUGH ULTRASOUND

TCD and transcranial color-coded doppler

TCD and transcranial color-coded Doppler (TCCD) are widely used tools for evaluating cerebral hemodynamics by measuring blood flow velocities in the major arteries of the circle of Willis. These techniques provide valuable, real-time data on CBF velocity and associated pathophysiological states.

Technical notes and procedure for TCD

A low frequency (2 MHz) pulsed Doppler probe is used to penetrate the cranial bones. The Acoustic Windows includes: (1) Transtemporal window: Located above the zygomatic arch, allowing access to the middle cerebral artery (MCA), anterior cerebral artery, and posterior cerebral artery; (2) Suboccipital window: Accesses the vertebrobasilar system, including the basilar artery and vertebral arteries; (3) Orbital window: Used to assess the ophthalmic artery and carotid siphon; and (4) Submandibular window: Allows direct measurement of flow in the extracranial internal carotid artery. The patient should lie supine or in a semi-recumbent position with minimal head movement. For the suboccipital window, the head is flexed slightly forward. Blood flow velocities are recorded at multiple depths (typically 30-65 mm for

MCA) in spectral waveform format. Peak systolic velocity (SFV), end-diastolic flow velocity (DFV), and mean flow velocity (MFV) are calculated. Pulsatility index, resistance index[26], and Lindegaard index[27] are derived from these measurements to assess vascular resistance, vasospasm, and other hemodynamic changes.

Technical notes and procedure for TCCD

TCCD combines Doppler and B-mode imaging to provide both hemodynamic and anatomical visualization of intracranial vessels. A 2-5 MHz phased-array transducer is used. Real-time vessel visualization, facilitating better localization. Ability to measure vessel diameter dynamically, enabling more accurate CBF estimation. The same acoustic windows as TCD are used, but TCCD provides color-coded maps of blood flow superimposed on grayscale images of the cranial anatomy. Vessels are identified based on their location, depth, and flow direction (*e.g.*, MCA shows flow toward the probe, while anterior cerebral artery shows flow away).

TCD and TCCD applications

The applications of TCD and TCCD includes: (1) Assessing vasospasm, intracranial stenosis, emboli detection, and cerebral autoregulation; (2) Estimation of ICP and CPP in neurocritical care settings; (3) Right to left shunting identification (bubble test); and (4) Facilitating simultaneous measurement of flow velocity and vessel diameter for precise CBF calculations.

TCD derived indexes and formulas

Both devices allows to measure blood flow velocities in the Willies circle or polygon main arteries in each cardiac cycle (Figure 6A). An important number of indexes and formulas derivate from that original measurement have been developed: (1) Gosling's pulsatility index (SFV - DFV/MFV): Represents the degree of variability of speed throughout the cardiac cycle, It depends on the peripheral resistance; (2) Pourcelot's Resistance index (SFV - DFV/SFV)[26]: Provides information about the resistance to blood flow within the vessel being examined. A higher resistance index indicates greater resistance to blood flow, which can be indicative of vascular pathology such as stenosis (narrowing) or occlusion (blockage) within the vessel. Conversely, a lower resistance index suggests less resistance to blood flow, which may be normal or indicative of increased perfusion; (3) Lindergaard Index (MFV in MCA/MFV in ICA)[27]: The ratio of the MFV in the MCA to the MFV in the internal carotid artery. An index greater than 3 is often interpreted as an indicator of cerebral vasospasm; (4) Bellner *et al*'s formula[28] for ICP estimation: ICP = 10.93 × pulsatility index - 1.28; (5) Belfort *et al*'s formula[29] for CPP estimation: CPP = (MFV/DFV) × (MAP - diastolic arterial pressure), where both in MCA; (6) Czyosnika formula for CPP estimation[30]: CPP = MAP × (DFV/MFV) + 14; and (7) CBF estimation: CBF (in ml/minutes) = MFV × π × (vessel diameter/2)^2 × 60, where MFV = MFV in MCA (in cm/second), vessel diameter = diameter of the cerebral artery (cm).

The CBF formula has been validated in two notable studies. Miyazawa *et al*[31] investigated the relationship between MCA MFV measured by TCD and CBF measured by single positron emission computed tomography imaging, using a three-dimensional stereotaxic region of interest template program. To account for variations in MCA cross-sectional area on brain blood flow estimation, they calculated MCA blood flow as the product of MCA MFV and MCA cross-sectional area, with MCA cross-sectional area estimated by magnetic resonance angiography. Their key findings demonstrated that TCD-measured brain blood flow indices, including MCA DFV and MFV, correlated significantly with total brain blood flow measured *via* standard single positron emission computed tomography. Moreover, this correlation improved when MCA blood flow, calculated as the product of MCA MFV and MCA cross-sectional area (from magnetic resonance angiography), was used as a TCD-derived index of brain blood flow. Jarrett *et al*[32] studied healthy volunteers to evaluate MCA diameter and flow velocities using TCCD, both with and without pharmaceutically induced vasodilation using nitroglycerin. This study provided valuable methodological insights, confirming real-time changes in MCA diameter during vasodilation. Their findings highlighted a robust approach to measuring both MCA flow velocity and diameter simultaneously, facilitating more accurate assessments of MCA blood flow.

Optic nerve sheath diameter

Optic nerve sheath diameter (ONSD) ultrasound has become a reliable, non-invasive technique for estimating ICP. Technical notes, usefulness and interpretation are published elsewhere but we recommend the last published systematic review[33] and review[34], which suggest the following guidelines: (1) Equipment and probe selection: A high-frequency (7-12 MHz) linear array transducer is typically used to ensure high-resolution images of the optic nerve; (2) Patient preparation: The patient is positioned supine with the head in a neutral position. The eyes should be closed, and sterile gel is applied over the eyelid. Light pressure is applied to avoid distortion of the underlying structures; (3) Technique: The probe is placed transversely over the closed eyelid, ensuring alignment with the optic nerve axis. The optic nerve is visualized posterior to the globe, appearing as a hypoechoic structure bordered by hyperechoic sheaths. The ONSD is measured 3 mm posterior to the globe, perpendicular to the optic nerve axis, and represents the widest diameter of the sheath; (4) Measurement interpretation: ONSD values greater than 5, 6 mm in adults typically indicate elevated ICP, although thresholds may vary based on clinical context and population. ONSD measurements are incorporated into several formulas of which we recommended the one developed by Lochner *et al*[35]: ICP = (ONSD - 3.7242)/0.128 mmHg; and (5) Applications: Monitoring ICP in TBI, subarachnoid hemorrhage, and other neurocritical conditions. Serving as a surrogate marker for non-invasive monitoring when invasive techniques (*e.g.*, intraventricular catheter) are contraindicated.

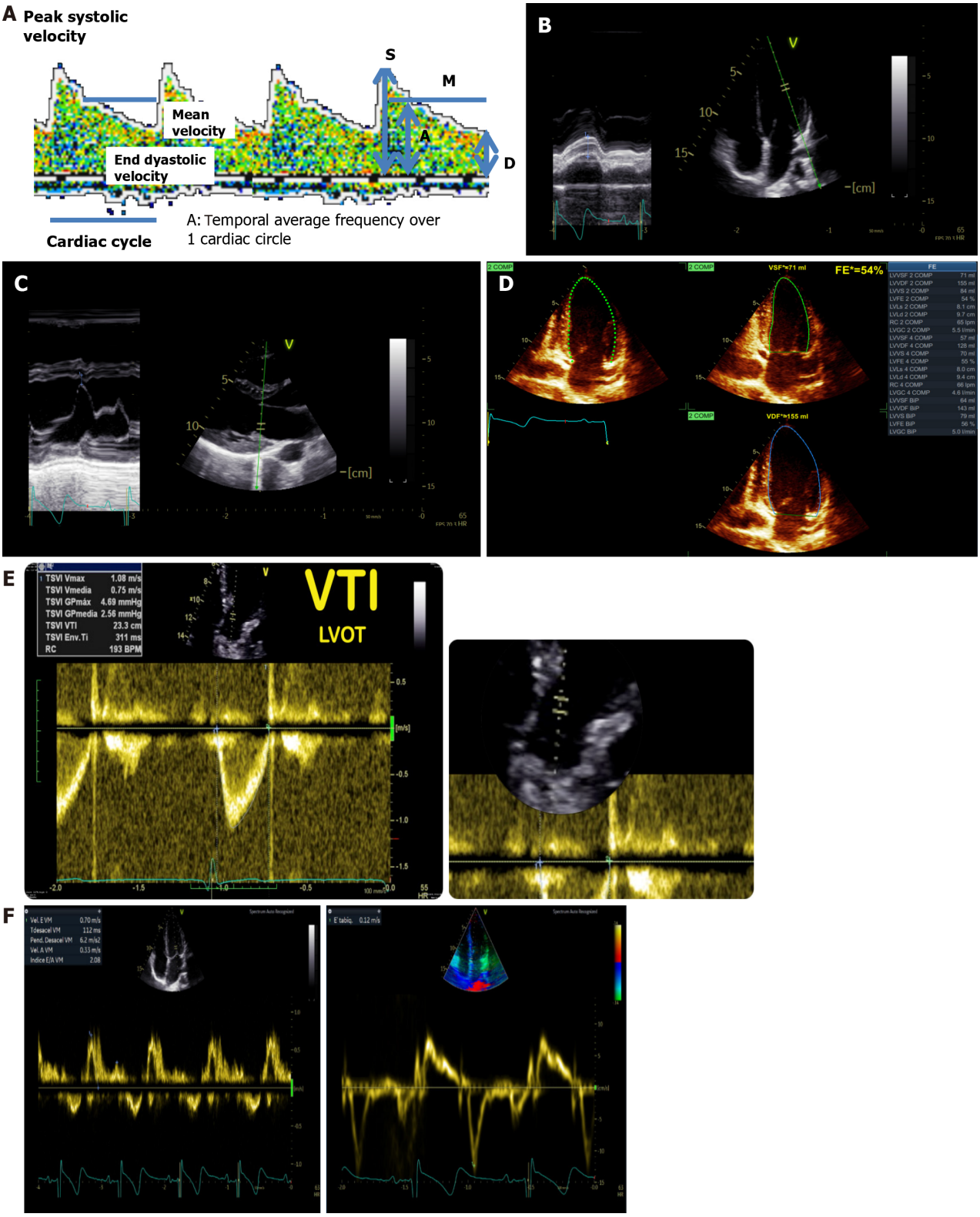

Figure 6 Assessment of cardio-cerebral coupling through ultrasound. A: Transcranial Doppler spectrum real measurements; B: Mitral annulus plane systolic excursion measurements; C: E point septal separation; D: Ejection fraction by biplane Simpson's method; E: Left ventricular outflow tract velocity time integral measurement; F: Transmitral Doppler. Left: Normal biphasic morphology, showing distinct E and A waves. Right: Normal triphasic morphology, with the addition of an L wave observed between the E and A waves. LVOT VTI: Left ventricular outflow tract velocity time.

Echocardiographic considerations in CCC

Left ventricular systolic function (LVSF) and left ventricular diastolic function (LVDF) assessment is fundamental in managing patients with acute cerebral pathology. Echocardiography performed in this context often differs in scope and objectives from that performed by specialized cardiologists. POCUS echocardiography focuses on rapid, bedside evaluations to answer specific clinical questions, such as assessing CO, detecting significant systolic dysfunction, or

identifying potential causes of hemodynamic instability. In contrast, specialized cardiology echocardiography provides a more comprehensive evaluation, employing advanced modalities like three-dimensional imaging, myocardial strain analysis, or transesophageal echocardiography to diagnose and monitor complex cardiac pathologies. This section outlines key echocardiographic methods for evaluating cardiac function, with a focus on practical, reproducible techniques that align with the principles of CCC.

LVSF

Evaluating LVSF in critically ill patients can be challenging due to poor acoustic windows and the supine positioning often required in intensive care. Although contractility is not synonymous with systolic function, these terms are often used interchangeably in clinical practice for simplicity. The assessment of LVSF typically begins with visual estimation, which provides a rapid differentiation between normal and significantly impaired function - a crucial distinction in critical care settings. Quantitative methods are then used to assign numerical values to LVSF, which should align with visual impressions.

Key echocardiographic methods for LVSF evaluation includes: (1) Mitral annulus plane systolic excursion (Figure 6B): Mitral annulus plane systolic excursion evaluates the motion of the mitral annulus toward the apex during systole, reflecting subendocardial fiber function. Using the M-mode in the apical four-chamber view, measure the excursion of the mitral annulus (septal and lateral) from valley to peak [normal values ≥ 16 mm (lateral annulus) and ≥ 10 mm (septal annulus), simple, reproducible, and less affected by interobserver variability, making it ideal for bedside assessments]; (2) E-point septal separation (Figure 6C): E-point septal separation measures the distance between the anterior mitral leaflet's E-point and the interventricular septum during early diastole. In the parasternal long-axis view, activate M-mode at the level of the anterior mitral leaflet and measure the minimal separation distance (normal value ≤ 7 mm, provides a quick estimate of LVSF, particularly in resource-limited settings); (3) Ejection fraction by Biplane Simpson's method (Figure 6D) : This gold-standard method calculates ejection fraction based on ventricular volumes derived from the apical four- and two-chamber views. Trace endocardial borders at end-diastole and end-systole in both views and calculate ejection fraction as the percentage of volume ejected. While widely used, this method is sensitive to loading conditions and may underestimate LVSF in low afterload states (*e.g.*, septic shock); (4) Myocardial strain (speckle tracking): Measures myocardial deformation (strain) over time using two-dimensional echocardiography. Provides angle-independent, precise evaluation of myocardial contractility, especially in patients with regional wall motion abnormalities or septic shock; and (5) Left ventricular outflow tract (LVOT) velocity time integral (VTI, Figure 6E): Combines LVOT diameter and VTI to estimate stroke volume using the cylinder volume formula: SV = π × (2 LVOT diameter) 2 × VTI. Use pulsed Doppler at the LVOT level in the apical five-chamber view. Enables indirect assessment of cerebral perfusion by correlating stroke volume and CO with CBF. Particularly useful in patients supported by extracorporeal membrane oxygenation, as demonstrated by Wang *et al*[36].

LVDF

LVDF ensures adequate ventricular filling while maintaining normal atrial pressures at rest and during physiological stress. Its assessment is particularly relevant in patients presenting with dyspnea, heart failure with preserved ejection fraction, or suspected diastolic dysfunction. Key echocardiographic methods for LVDF evaluation includes: (1) Transmitral Doppler (Figure 6F): Evaluates blood flow velocities through the mitral valve during diastole. Using pulsed Doppler at the mitral valve tips in the apical four-chamber view, measure E wave (early diastolic filling velocity, normal: 60-100 cm/second), A wave (late diastolic filling velocity, normal: approximately 50 cm/second), E/A ratio (reflects diastolic relaxation and left atrial function), and E wave deceleration time (time from the E wave peak to baseline, normal: 150-240 ms). Assists in diagnosing diastolic dysfunction and differentiating cardiac dyspnea from pulmonary causes; and (2) Tissue Doppler imaging of the mitral annulus: Assesses myocardial velocities at the mitral annulus during systole and diastole. Place the sample volume 1 cm above the mitral leaflet insertion in the apical four-chamber view to record e' wave (early diastolic annular velocity, septal > 7 cm/second, lateral > 10 cm/second) and E/e' ratio (indicates filling pressures, normal E/e' < 8, elevated E/e' > 15). Highly reproducible and less preload-dependent, making it a robust marker of diastolic dysfunction.

Integration of echocardiography in CCC

Echocardiography plays a pivotal role in understanding CCC by linking CO and systemic hemodynamics to cerebral perfusion. Specifically: (1) LVSF and LVDF assessments: Help identify cardiac contributions to cerebral hypoperfusion in conditions like subarachnoid hemorrhage and TBI; (2) LVOT VTI and TCD/TCCD: Offers complementary insights into stroke volume and CBF, enabling a more comprehensive evaluation of cardio-cerebral dynamics; and (3) Myocardial strain and advanced imaging: Expand the diagnostic scope, particularly in critical care and complex pathologies.

CCC IN HEALTH AND DISEASE

The concept of CCC is supported by the pathophysiological mechanisms described earlier, with exercise providing one of the clearest demonstrations of this phenomenon. During exercise, the skeletal muscles demand increased oxygen and energy, leading to local vasodilation. If left uncontrolled, this vasodilation could result in systemic circulatory collapse, particularly compromising cerebral circulation. However, mechanisms such as the exercise pressor reflex, metabolic reflexes, and central command prevent this outcome (Figure 4). Conversely, in activities like mindfulness meditation, where there is minimal muscle activity, CBF paradoxically increases[37]. Studies suggest this response is mediated by

simultaneous sympathetic and parasympathetic activation during meditation[38-40], corresponding to the pathways highlighted in Figure 4.

Cardio-cerebral uncoupling in disease

Cardio-cerebral uncoupling becomes evident in conditions such as type II diabetes complicated by heart failure. Pinna *et al*[41] demonstrated impaired coupling during simultaneous metaboreflex activation and mental task execution, using near-infrared spectroscopy to measure CBF and impedance cardiography to assess central hemodynamics. In diabetics, cerebral oxygenation and CBF were significantly reduced compared to healthy controls. The Cushing reflex, described in 1901, characterized by arterial hypertension, bradycardia, and respiratory changes secondary to elevated ICP, also reflects disrupted CCC. Dickinson's review[42] of the reflex noted that while the full response occurs during acute ICP elevation, bradycardia is absent in gradual ICP increases, suggesting a last-resort protective mechanism for a severely ischemic brain. Studies by Reis *et al*[43,44], Guyenet[45], and Schmidt *et al*[46] confirmed the role of the rostral ventrolateral medulla in the sympathetic activation of the reflex, potentially working synergistically with parasympathetic responses to enhance stroke volume through prolonged diastolic filling time.

TCD in monitoring CCC

Using the TCD simulator developed by Aaslid (https://www.transcranial.com/edu/index.html), the progressive failure of CCC can be simulated in scenarios such as TBI, intracranial hemorrhage, or ischemic stroke leading to acute intracranial hypertension. These conditions show decreasing CBF velocities, increasing pulsatility index, and declining DFV, eventually progressing to pulsatile flow or isolated systolic spikes and culminating in cerebral circulatory arrest (Figure 7A). In cases of primary cardiac dysfunction, such as ventricular fibrillation or cardiogenic shock, cardio-cerebral autoregulation may also fail, resulting in cerebral circulatory arrest (Figure 7B).

Ultrasound-guided protocols for cardio-cerebral resuscitation

Building on these observations, our pilot study demonstrated the utility of TCD-guided resuscitation in traumatic and non-traumatic comatose patients[47]. Patients presenting with DFV < 20 cm/second or pulsatility index > 1.4 were treated with a protocol starting with a 1-liter saline infusion, followed by noradrenaline titration if no response was observed. Persistent oscillating flow or DFV < 20 cm/second was associated with 100% mortality, while normal TCD findings correlated with survival. Based on these findings, we developed the ultrasound-guided cardio-cerebral resuscitation protocol[48] (ReCCUs for its Spanish acronym, Figure 7C), which integrates TCD and transthoracic echocardiography into the Advanced Trauma Life Support® A (airway), B (breathing), C (circulation), D (disability), E (exposure) framework. This protocol aims to optimize cardiac function and ensure adequate CBF during resuscitation.

Ultrasound-guided brain injury treatment protocol

For resource-limited settings, we developed the ultrasound-guided brain injury treatment protocol (TTECUs for its Spanish acronym, Figure 7D). This protocol incorporates: (1) ICP estimation: Using ONSD measurements and the Bellner formula; (2) CPP estimation: Using the Belfort formula; and (3) Detection of midline shift and space-occupying lesions: Using mesencephalic ultrasound. This protocol supplements the consensus-based management protocol for severe TBI in regions lacking access to invasive monitoring tools[49]. Both the ReCCUs and TTECUs protocols are currently being tested in 15 centers across Argentina, Ecuador, Colombia, Bolivia, and Costa Rica. Preliminary results are anticipated by December 2025.

Ventilator-associated brain injury

An emerging example of impaired CCC is the concept of ventilator-associated brain injury[50], which refers to the development of primary brain injury in patients without preexisting neurological conditions undergoing mechanical ventilation. Our research aligns with this concept and attempts to explain it using the framework of the complex vasodilator cascade (Figure 3B) and NVU impairment. In two studies currently under review, we identified mechanical ventilation as a significant contributor to cognitive impairment following severe respiratory failure. One of these studies, which received recognition from the Argentine National Academy of Medicine, analyzed a cohort of neuro-Corona Virus Infectious Disease-2019 patients with severe respiratory failure (Pa/FiO_2 < 200) meeting the Berlin criteria for acute respiratory distress syndrome (ARDS). Patients were treated with either mechanical ventilation or non-invasive ventilation. Among those receiving mechanical ventilation, 75% of survivors developed post-intensive care syndrome (PICS), with cognitive impairment as the most prominent feature, while no cases of PICS were observed in the non-invasive ventilation group. In the second study, we prospectively examined a cohort of 56 Corona Virus Infectious Disease-2019 patients with severe respiratory failure (Pa/FiO_2 < 200) meeting the Berlin ARDS criteria, evaluating ICP using ONSD. Elevated ICP was detected in 67% of mechanically ventilated patients, and 75% of these patients exhibited PICS at ICU discharge.

These findings can be understood by revisiting Figure 3B, which highlights how ARDS triggers a cascade of systemic changes - hypoxia, fever, hypocarbia, acidosis, hypotension, and increased metabolic demands - that initiate direct vasodilation and lead to intracranial hypertension. Additionally, mechanical ventilation and pulmonary stiffness further exacerbate ICP elevation by increasing intrathoracic pressure and impairing jugular venous return. Other contributing mechanisms include sympathetic reflexes induced by alveolar and myocardial damage, systemic endothelial inflammation, and the absence of muscle activity, which disrupts the muscle metaboreflex and reduces neurotrophic factor secretion.

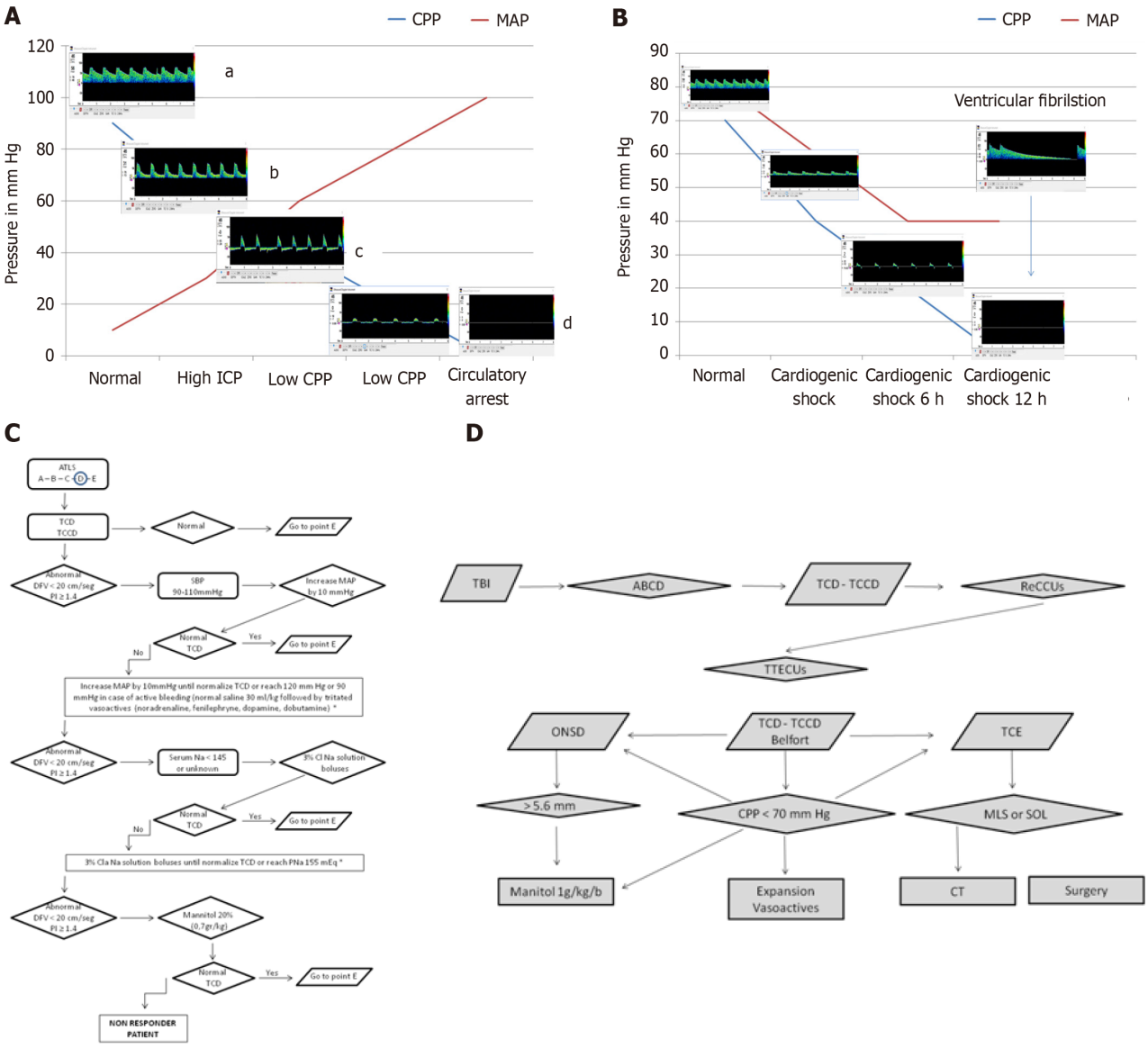

Figure 7 Cardio-cerebral coupling in health and disease. A: Changes in flow velocities as cerebral perfusion pressures (CPP) decreases due to increasing intracranial pressure (ICP). [a]Normal flow: CPP at 90 mmHg and ICP at 10 mmHg ensures adequate cerebral perfusion with normal diastolic flow velocity (DFV) and pulsatility index. [b]High ICP: An increase in cerebral vascular resistance due to elevated ICP leads to compromised DFV and elevated pulsatility index. [c]Low CPP: Further increases in cerebral vascular resistance, coupled with low CPP, progress to reverberant flow. If sustained, this can evolve into small systolic spikes or complete flow absence. [d]Cerebral circulatory arrest (CCA): The presence of reverberant flow or systolic spikes for more than 30 minutes is indicative of CCA, as defined by most brain death criteria; B: Changes in flow velocities as cardiogenic shock progresses. Early phase: Cardiogenic shock leads to a gradual decrease in all flow velocities, with a more pronounced reduction in DFV. Reverberant flow: After 6 hours, the typical pattern of reverberant flow emerges, characterized by oscillating flow without effective forward perfusion. CCA: Sustained reverberant flow or the appearance of complete flow absence (total CCA) is observed. Prolonged ventricular fibrillation can also result in this pattern. The presence of reverberant flow for more than 30 minutes is a reliable indicator of CCA, as defined by most brain death legislations; C: The ultrasound-guided cardio-cerebral resuscitation protocol. The Advanced Trauma Life Support® systematic approach includes airway, breathing, circulation, disability, and exposure; D: The ultrasound-guided brain injury treatment protocol. Following initial resuscitation using the ultrasound-guided brain injury treatment protocol, CPP is assessed using Belfort's formula, ICP is estimated *via* optic nerve sheath diameter, and brain morphology is evaluated using B-mode transcranial ultrasound. If CPP < 70 mmHg, fluid expansion and vasoactive agents are immediately initiated. Simultaneously, optic nerve sheath diameter is measured. If ICP is elevated, a mannitol bolus is administered. If transcranial ultrasound reveals a midline shift or space-occupying lesion, the patient is immediately transferred to the computed tomography suite for surgical evaluation. This protocol ensures a systematic, ultrasound-guided approach to managing traumatic brain injury and optimizing cerebral perfusion. CPP: Cerebral perfusion pressures; ICP: Intracranial pressure; ATLS: Advanced Trauma Life Support®; TCD: Transcranial Doppler; TCCD: Transcranial color-coded Doppler; DFV: End-diastolic flow velocity; PI: Pulsatility index; SBP: Systolic blood pressure; MAP: Mean arterial pressure; TBI: Traumatic brain injury; ReCCUs: Ultrasound-guided cardio-cerebral resuscitation protocol; TTECUs: Ultrasound-guided brain injury treatment protocol; ONSD: Optic nerve sheath diameter; TCE: B-mode transcranial ultrasound; MLS: Midline shift; SOL: Space-occupying lesion; CT: Computed tomography.

CONCLUSION

The concept of CCC integrates a deep understanding of the pathophysiological mechanisms governing CBF, blood pressure, and CO. This complex interplay is essential for maintaining homeostasis and is profoundly influenced by systemic and cerebral hemodynamics. Ultrasound-based techniques, such as TCD, TCCD, ONSD measurements, and echocardiography, provide a versatile, non-invasive toolkit for assessing these mechanisms in both health and disease. Throughout this review, we have explored the multifaceted nature of CCC, delving into its role in exercise, pathologies such as ARDS and heart failure, and scenarios of disrupted coupling like ventilator-associated brain injury. We have emphasized the value of ultrasound-based protocols, such as ReCCUs and TTECUs, as practical and scalable tools for bedside monitoring and intervention, particularly in resource-limited settings. These protocols exemplify the potential of POCUS to bridge gaps in critical care by offering real-time insights into cardio-cerebral dynamics. Despite these advancements, significant research gaps remain. Future studies should focus on standardizing ultrasound protocols, validating new indices for clinical application, and further elucidating the mechanisms linking systemic and cerebral hemodynamics. Neurosonology and echocardiography will undoubtedly continue to play a pivotal role in this evolving field, guiding both research and clinical practice toward optimizing outcomes for patients with cardio-cerebral dysregulation.

FOOTNOTES

Author contributions: Previgliano IJ, Aboumarie HS, Tamagnone FM, Merlo PM, Sosa FA, Feijoo J, and Carruega MC contributed to concept development, first manuscript draft and final manuscript review; Previgliano IJ contributed to pathophysiology and final manuscript edition; Aboumarie HS contributed to English language review; Previgliano IJ and Aboumarie HS contributed equally as co-first authors; Merlo PM contributed to echocardiography and cardiovascular pathophysiology; Sosa FA, Carruega MC, and Feijoo J contributed to bibliographical search and handling; Carruega MC contributed to reference adaptation to journal standards; Feijoo J contributed to graphics edition.

Conflict-of-interest statement: All the authors report no relevant conflicts of interest for this article.

Open Access: This article is an open-access article that was selected by an in-house editor and fully peer-reviewed by external reviewers. It is distributed in accordance with the Creative Commons Attribution NonCommercial (CC BY-NC 4.0) license, which permits others to distribute, remix, adapt, build upon this work non-commercially, and license their derivative works on different terms, provided the original work is properly cited and the use is non-commercial. See: https://creativecommons.org/Licenses/by-nc/4.0/

Country of origin: Argentina

ORCID number: Ignacio J Previgliano 0000-0003-2114-6538; Hatem Soliman Aboumarie 0000-0002-3254-6820; Francisco M Tamagnone 0000-0002-2166-5007; Pablo M Merlo 0000-0001-6413-1964; Fernando A Sosa 0000-0002-4865-1895; Jose Feijoo 0000-0002-5074-728X; Maria C Carruega 0000-0003-3329-4829.

S-Editor: Wei YF
L-Editor: A
P-Editor: Guo X

REFERENCES

1 **Castle-Kirszbaum M**, Parkin WG, Goldschlager T, Lewis PM. Cardiac Output and Cerebral Blood Flow: A Systematic Review of Cardio-Cerebral Coupling. *J Neurosurg Anesthesiol* 2022; **34**: 352-363 [PMID: 33782372 DOI: 10.1097/ANA.0000000000000768] [FullText]
2 **Langfitt TW**. Increased intracranial pressure. *Clin Neurosurg* 1969; **16**: 436-471 [PMID: 4981573 DOI: 10.1093/neurosurgery/16.cn_suppl_1.436] [FullText]
3 **Rosner MJ**, Newsome HH, Becker DP. Mechanical brain injury: the sympathoadrenal response. *J Neurosurg* 1984; **61**: 76-86 [PMID: 6726414 DOI: 10.3171/jns.1984.61.1.0076] [FullText]
4 **Rosner MJ**, Becker DP. Origin and evolution of plateau waves. Experimental observations and a theoretical model. *J Neurosurg* 1984; **60**: 312-324 [PMID: 6693959 DOI: 10.3171/jns.1984.60.2.0312] [FullText]
5 **Rosner MJ**. Introduction to cerebral perfusion pressure management. *Neurosurg Clin N Am* 1995; **6**: 761-773 [PMID: 8527917] [FullText]
6 **Becker DP**, Miller JD, Ward JD, Greenberg RP, Young HF, Sakalas R. The outcome from severe head injury with early diagnosis and intensive management. *J Neurosurg* 1977; **47**: 491-502 [PMID: 903803 DOI: 10.3171/jns.1977.47.4.0491] [FullText]
7 **Chan KH**, Dearden NM, Miller JD, Andrews PJ, Midgley S. Multimodality monitoring as a guide to treatment of intracranial hypertension after severe brain injury. *Neurosurgery* 1993; **32**: 547-52; discussion 552 [PMID: 8474645 DOI: 10.1227/00006123-199304000-00009] [FullText]
8 **Bouma GJ**, Muizelaar JP, Bandoh K, Marmarou A. Blood pressure and intracranial pressure-volume dynamics in severe head injury: relationship with cerebral blood flow. *J Neurosurg* 1992; **77**: 15-19 [PMID: 1607958 DOI: 10.3171/jns.1992.77.1.0015] [FullText]
9 **Carney N**, Totten AM, O'Reilly C, Ullman JS, Hawryluk GW, Bell MJ, Bratton SL, Chesnut R, Harris OA, Kissoon N, Rubiano AM, Shutter L, Tasker RC, Vavilala MS, Wilberger J, Wright DW, Ghajar J. Guidelines for the Management of Severe Traumatic Brain Injury, Fourth Edition. *Neurosurgery* 2017; **80**: 6-15 [PMID: 27654000 DOI: 10.1227/NEU.0000000000001432] [FullText]

10 **Roy CS**, Sherrington CS. On the Regulation of the Blood-supply of the Brain. *J Physiol* 1890; **11**: 85-158.17 [PMID: 16991945 DOI: 10.1113/jphysiol.1890.sp000321] [FullText]

11 **Hamner JW**, Tan CO, Lee K, Cohen MA, Taylor JA. Sympathetic control of the cerebral vasculature in humans. *Stroke* 2010; **41**: 102-109 [PMID: 20007920 DOI: 10.1161/STROKEAHA.109.557132] [FullText]

12 **Sándor P**. Nervous control of the cerebrovascular system: doubts and facts. *Neurochem Int* 1999; **35**: 237-259 [PMID: 10458655 DOI: 10.1016/s0197-0186(99)00067-4] [FullText]

13 **Claassen JAHR**, Thijssen DHJ, Panerai RB, Faraci FM. Regulation of cerebral blood flow in humans: physiology and clinical implications of autoregulation. *Physiol Rev* 2021; **101**: 1487-1559 [PMID: 33769101 DOI: 10.1152/physrev.00022.2020] [FullText]

14 **Alam M**, Smirk FH. Observations in man upon a blood pressure raising reflex arising from the voluntary muscles. *J Physiol* 1937; **89**: 372-383 [PMID: 16994867 DOI: 10.1113/jphysiol.1937.sp003485] [FullText]

15 **Kaufman MP**, Hayes SG. The exercise pressor reflex. *Clin Auton Res* 2002; **12**: 429-439 [PMID: 12598947 DOI: 10.1007/s10286-002-0059-1] [FullText]

16 **Teixeira AL**, Vianna LC. The exercise pressor reflex: An update. *Clin Auton Res* 2022; **32**: 271-290 [PMID: 35727398 DOI: 10.1007/s10286-022-00872-3] [FullText]

17 **Crisafulli A**. The Impact of Cardiovascular Diseases on Cardiovascular Regulation During Exercise in Humans: Studies on Metaboreflex Activation Elicited by the Post-exercise Muscle Ischemia Method. *Curr Cardiol Rev* 2017; **13**: 293-300 [PMID: 28782491 DOI: 10.2174/1573403X13666170804165928] [FullText]

18 **Smith KJ**, Ainslie PN. Regulation of cerebral blood flow and metabolism during exercise. *Exp Physiol* 2017; **102**: 1356-1371 [PMID: 28786150 DOI: 10.1113/EP086249] [FullText]

19 **Teixeira AL**, Fernandes IA, Vianna LC. Cardiovascular Control During Exercise: The Connectivity of Skeletal Muscle Afferents to the Brain. *Exerc Sport Sci Rev* 2020; **48**: 83-91 [PMID: 32000180 DOI: 10.1249/JES.0000000000000218] [FullText]

20 **White M**, Bruce R. The role of muscle mechano and metaboreflexes in the control of ventilation: breathless with (over) excitement? *Exp Physiol* 2020; **105**: 2250-2253 [PMID: 32978846 DOI: 10.1113/EP088460] [FullText]

21 **Harder DR**, Zhang C, Gebremedhin D. Astrocytes function in matching blood flow to metabolic activity. *News Physiol Sci* 2002; **17**: 27-31 [PMID: 11821533 DOI: 10.1152/physiologyonline.2002.17.1.27] [FullText]

22 **Iadecola C**. Neurovascular regulation in the normal brain and in Alzheimer's disease. *Nat Rev Neurosci* 2004; **5**: 347-360 [PMID: 15100718 DOI: 10.1038/nrn1387] [FullText]

23 **Abbott NJ**, Rönnbäck L, Hansson E. Astrocyte-endothelial interactions at the blood-brain barrier. *Nat Rev Neurosci* 2006; **7**: 41-53 [PMID: 16371949 DOI: 10.1038/nrn1824] [FullText]

24 **Iadecola C**. The overlap between neurodegenerative and vascular factors in the pathogenesis of dementia. *Acta Neuropathol* 2010; **120**: 287-296 [PMID: 20623294 DOI: 10.1007/s00401-010-0718-6] [FullText]

25 **Brightman MW**, Kadota Y. Nonpermeable and permeable vessels of the brain. *NIDA Res Monogr* 1992; **120**: 87-107 [PMID: 1501694] [Full Text]

26 **Planiol T**, Pourcelot L, Itti R. [The carotid and cerebral circulations. Advances in its study by external physical methods. Principles, normal recordings, adopted parameters]. *Nouv Presse Med* 1973; **2**: 2451-2456 [PMID: 4748647] [FullText]

27 **Lindegaard KF**, Nornes H, Bakke SJ, Sorteberg W, Nakstad P. Cerebral vasospasm after subarachnoid haemorrhage investigated by means of transcranial Doppler ultrasound. *Acta Neurochir Suppl (Wien)* 1988; **42**: 81-84 [PMID: 3055838 DOI: 10.1007/978-3-7091-8975-7_16] [Full Text]

28 **Bellner J**, Romner B, Reinstrup P, Kristiansson KA, Ryding E, Brandt L. Transcranial Doppler sonography pulsatility index (PI) reflects intracranial pressure (ICP). *Surg Neurol* 2004; **62**: 45-51; discussion 51 [PMID: 15226070 DOI: 10.1016/j.surneu.2003.12.007] [FullText]

29 **Belfort MA**, Tooke-Miller C, Varner M, Saade G, Grunewald C, Nisell H, Herd JA. Evaluation of a noninvasive transcranial Doppler and blood pressure-based method for the assessment of cerebral perfusion pressure in pregnant women. *Hypertens Pregnancy* 2000; **19**: 331-340 [PMID: 11118407 DOI: 10.1081/prg-100101995] [FullText]

30 **Schmidt EA**, Czosnyka M, Gooskens I, Piechnik SK, Matta BF, Whitfield PC, Pickard JD. Preliminary experience of the estimation of cerebral perfusion pressure using transcranial Doppler ultrasonography. *J Neurol Neurosurg Psychiatry* 2001; **70**: 198-204 [PMID: 11160468 DOI: 10.1136/jnnp.70.2.198] [FullText]

31 **Miyazawa T**, Shibata S, Nagai K, Hirasawa A, Kobayashi Y, Koshiba H, Kozaki K. Relationship between cerebral blood flow estimated by transcranial Doppler ultrasound and single-photon emission computed tomography in elderly people with dementia. *J Appl Physiol (1985)* 2018; **125**: 1576-1584 [PMID: 30188796 DOI: 10.1152/japplphysiol.00118.2018] [FullText]

32 **Jarrett CL**, Shields KL, Broxterman RM, Hydren JR, Park SH, Gifford JR, Richardson RS. Imaging transcranial Doppler ultrasound to measure middle cerebral artery blood flow: the importance of measuring vessel diameter. *Am J Physiol Regul Integr Comp Physiol* 2020; **319**: R33-R42 [PMID: 32401627 DOI: 10.1152/ajpregu.00025.2020] [FullText]

33 **Lau T**, Ahn JS, Manji R, Kim DJ. A Narrative Review of Point of Care Ultrasound Assessment of the Optic Nerve in Emergency Medicine. *Life (Basel)* 2023; **13**: 531 [PMID: 36836888 DOI: 10.3390/life13020531] [FullText]

34 **Berhanu D**, Ferreira JC, Abegão Pinto L, Aguiar de Sousa D, Lucas Neto L, Tavares Ferreira J. The role of optic nerve sheath ultrasonography in increased intracranial pressure: A systematic review and meta analysis. *J Neurol Sci* 2023; **454**: 120853 [PMID: 37925899 DOI: 10.1016/j.jns.2023.120853] [FullText]

35 **Lochner P**, Czosnyka M, Naldi A, Lyros E, Pelosi P, Mathur S, Fassbender K, Robba C. Optic nerve sheath diameter: present and future perspectives for neurologists and critical care physicians. *Neurol Sci* 2019; **40**: 2447-2457 [PMID: 31367861 DOI: 10.1007/s10072-019-04015-x] [FullText]

36 **Wang M**, Li L, Tan YD. Transcranial Doppler Ultrasound for Monitoring the Cerebral Hemodynamic Changes and Prognosticating Outcomes in Venoarterial Extracorporeal Membrane-Oxygenated Patients. *Int J Clin Pract* 2022; **2022**: 2912477 [PMID: 36052306 DOI: 10.1155/2022/2912477] [FullText]

37 **Pommy J**, Smart CM, Bryant AM, Wang Y. Three potential neurovascular pathways driving the benefits of mindfulness meditation for older adults. *Front Aging Neurosci* 2023; **15**: 1207012 [PMID: 37455940 DOI: 10.3389/fnagi.2023.1207012] [FullText]

38 **Park C**, Youn I, Han S. Single-lead ECG based autonomic nervous system assessment for meditation monitoring. *Sci Rep* 2022; **12**: 22513 [PMID: 36581715 DOI: 10.1038/s41598-022-27121-x] [FullText]

39 **Nijjar PS**, Puppala VK, Dickinson O, Duval S, Duprez D, Kreitzer MJ, Benditt DG. Modulation of the autonomic nervous system assessed

through heart rate variability by a mindfulness based stress reduction program. *Int J Cardiol* 2014; **177**: 557-559 [PMID: 25179555 DOI: 10.1016/j.ijcard.2014.08.116] [FullText]

40 **Léonard A**, Clément S, Kuo CD, Manto M. Changes in Heart Rate Variability During Heartfulness Meditation: A Power Spectral Analysis Including the Residual Spectrum. *Front Cardiovasc Med* 2019; **6**: 62 [PMID: 31139634 DOI: 10.3389/fcvm.2019.00062] [FullText]

41 **Pinna V**, Doneddu A, Roberto S, Magnani S, Ghiani G, Mulliri G, Sanna I, Serra S, Hosseini Kakhak SA, Milia R, Fadda D, Lecis R, Guicciardi M, Crisafulli A. Combined mental task and metaboreflex impair cerebral oxygenation in patients with type 2 diabetes mellitus. *Am J Physiol Regul Integr Comp Physiol* 2021; **320**: R488-R499 [PMID: 33533319 DOI: 10.1152/ajpregu.00288.2020] [FullText]

42 **Dickinson CJ**. Reappraisal of the Cushing reflex: the most powerful neural blood pressure stabilizing system. *Clin Sci (Lond)* 1990; **79**: 543-550 [PMID: 2176941 DOI: 10.1042/cs0790543] [FullText]

43 **Reis DJ**, Golanov EV, Ruggiero DA, Sun MK. Sympatho-excitatory neurons of the rostral ventrolateral medulla are oxygen sensors and essential elements in the tonic and reflex control of the systemic and cerebral circulations. *J Hypertens Suppl* 1994; **12**: S159-S180 [PMID: 7769486] [FullText]

44 **Reis DJ**, Ruggiero DA, Morrison SF. The C1 area of the rostral ventrolateral medulla oblongata. A critical brainstem region for control of resting and reflex integration of arterial pressure. *Am J Hypertens* 1989; **2**: 363S-374S [PMID: 2574588] [FullText]

45 **Guyenet PG**. Neural structures that mediate sympathoexcitation during hypoxia. *Respir Physiol* 2000; **121**: 147-162 [PMID: 10963771 DOI: 10.1016/s0034-5687(00)00125-0] [FullText]

46 **Schmidt EA**, Despas F, Pavy-Le Traon A, Czosnyka Z, Pickard JD, Rahmouni K, Pathak A, Senard JM. Intracranial Pressure Is a Determinant of Sympathetic Activity. *Front Physiol* 2018; **9**: 11 [PMID: 29472865 DOI: 10.3389/fphys.2018.00011] [FullText]

47 **Tamagnone F**, Martínez E, Blejman SD, Rubianes JI, Previgliano IJ. A pilot study of transcranial Doppler-guided initial resuscitation of traumatic and non-traumatic comatose patients. *Minerva Anestesiol* 2014; **80**: 1012-1017 [PMID: 24463943] [FullText]

48 **Tamagnone FM**, Cheong I, Luna E, Previgliano I, Otero Castro V. Ultrasound-guided cerebral resuscitation in patients with severe traumatic brain Injury. *J Clin Monit Comput* 2023; **37**: 359-363 [PMID: 36454340 DOI: 10.1007/s10877-022-00954-7] [FullText]

49 **Chesnut RM**, Temkin N, Videtta W, Petroni G, Lujan S, Pridgeon J, Dikmen S, Chaddock K, Barber J, Machamer J, Guadagnoli N, Hendrickson P, Aguilera S, Alanis V, Bello Quezada ME, Bautista Coronel E, Bustamante LA, Cacciatori AC, Carricondo CJ, Carvajal F, Davila R, Dominguez M, Figueroa Melgarejo JA, Fillipi MM, Godoy DA, Gomez DC, Lacerda Gallardo AJ, Guerra Garcia JA, Zerain GF, Lavadenz Cuientas LA, Lequipe C, Grajales Yuca GV, Jibaja Vega M, Kessler ME, López Delgado HJ, Sandi Lora F, Mazzola AM, Maldonado RM, Mezquia de Pedro N, Martínez Zubieta JR, Mijangos Méndez JC, Mora J, Ochoa Parra JM, Pahnke PB, Paranhos J, Piñero GR, Rivadeneira Pilacuán FA, Mendez Rivera MN, Romero Figueroa RL, Rubiano AM, Saraguro Orozco AM, Silesky Jiménez JI, Silva Naranjo L, Soler Morejon C, Urbina Z. Consensus-Based Management Protocol (CREVICE Protocol) for the Treatment of Severe Traumatic Brain Injury Based on Imaging and Clinical Examination for Use When Intracranial Pressure Monitoring Is Not Employed. *J Neurotrauma* 2020; **37**: 1291-1299 [PMID: 32013721 DOI: 10.1089/neu.2017.5599] [FullText]

50 **Bassi T**, Taran S, Girard TD, Robba C, Goligher EC. Ventilator-associated Brain Injury: A New Priority for Research in Mechanical Ventilation. *Am J Respir Crit Care Med* 2024; **209**: 1186-1188 [PMID: 38526447 DOI: 10.1164/rccm.202401-0069VP] [FullText]

Published by **Baishideng Publishing Group Inc**
7041 Koll Center Parkway, Suite 160, Pleasanton, CA 94566, USA
Telephone: +1-925-3991568
E-mail: office@baishideng.com
Help Desk: https://www.f6publishing.com/helpdesk
https://www.wjgnet.com

© 2025 Baishideng Publishing Group Inc. All rights reserved.